Inorganic Chemistry

Article

pubs.acs.org/IC

2-(2-Hydroxyphenyl)benzimidazole-Based Four-Coordinate Boron-Containing Materials with Highly Efficient Deep-Blue Photoluminescence and Electroluminescence

Zhenyu Zhang, Houyu Zhang, Chuanjun Jiao, Kaiqi Ye, Hongyu Zhang,* Jingying Zhang,* and Yue Wang

State Key Laboratory of Supramolecular Structure and Materials, International Joint Research Laboratory of Nano-Micro Architecture Chemistry, College of Chemistry, Jilin University, Changchun 130012, P. R. China

Supporting Information

ABSTRACT: Two novel four-coordinate boron-containing emitters **1** and **2** with deep-blue emissions were synthesized by refluxing a 2-(2-hydroxyphenyl)benzimidazole ligand with triphenylborane or bromodibenzoborole. The boron chelation produced a new π-conjugated skeleton, which rendered the synthesized boron materials with intense fluorescence, good thermal stability, and high carrier mobility. Both compounds displayed deep-blue emissions in solutions with very high fluorescence quantum yields (over 0.70). More importantly, the samples showed identical fluorescence in the solution and solid states, and the efficiency was maintained at a high level (approximately 0.50) because of the bulky substituents between the boron atom and the benzimidazole unit, which can effectively separate the flat luminescent units. In addition, neat thin films composed of **1** or **2** exhibited high electron and hole mobility in the same order of magnitude 10^{-4}, as determined by time-of-flight. The fabricated electroluminescent devices that employed **1** or **2** as emitting materials showed high-performance deep-blue emissions with Commission Internationale de L'Eclairage (CIE) coordinates of (X = 0.15, Y = 0.09) and (X = 0.16, Y = 0.08), respectively. Thus, the synthesized boron-containing materials are ideal candidates for fabricating high-performance deep-blue organic light-emitting diodes.

INTRODUCTION

Organic π-conjugated materials with intense solid-state fluorescence have attracted much attention in recent years because of their potential applications in organic light-emitting diodes (OLEDs), organic solid-state lasers (OSLs), sensors, bioimages, and so on.[1] Among these materials, four-coordinate boron compounds have proven to be effective luminescent materials with wide applications.[2] The molecular structures of boron-containing materials can be easily modified for the desired properties by altering either the ligands or substituents on the boron atoms. Different ligands such as diaryl-β-diketone,[3] N-heterocycle-phenolate,[4] pyridylphenole,[5] hydroxyquinoline,[6] N-heterocyclophenole,[7] and other species[8] have been designed. The reaction of these ligands with organoborane reagents allows the easy synthesis of multitudinous four-coordinate boron-containing compounds. Red (R), green (G), and blue (B) emissions have been realized by structural modification, and certain boron materials even exhibit bright emissions in the solid state. The resulting π-conjugated structures can not only enhance the electron deficiency of the π-system through intramolecular electron delocalization but also intensify the emission by constraining molecular rotations. Therefore, luminescent π-conjugated materials bearing four-coordinate boron moieties have been widely employed as emitting or/and electron-transporting layers in OLEDs and some of them perform well.

Our group has been continuously interested in designing novel boron-containing π-conjugated systems for fabricating high-performance OLEDs and found that boron compounds that possess a ladder-type π-framework after boron chelation are ideal candidates. Boron-bridged ladder-type molecules with conjugation length that ranges from four to seven rings have been synthesized in our laboratory for this purpose.[9] The structural rigidity of the flat ladder-type π-skeleton endows these materials with intense fluorescence, good thermal stability, and high charge mobility. Electroluminescent devices that employ these boron materials as emitters show RGB electroluminescence (EL) with very high brightness and efficiencies. However, deep-blue EL with Commission Internationale de L'Eclairage (CIE) coordinates (X, Y) below 0.15 and 0.10, respectively, has not yet been achieved based on four-coordinate boron-containing materials. The achievement of CIE_Y below 0.10 requires the major emission profiles located in the deep-blue region. Therefore, not only emission peaks but also spectral bandwidths are important for realizing deep-blue luminescence.[10] Certain rigid π-conjugated compounds such as anthracene or pyrene derivatives show intense deep-blue fluorescence in a dispersed state; however, their emissions are significantly red-shifted after aggregation, accompanied by reduced fluorescence quantum yield, because of strong

Received: November 25, 2014
Published: February 25, 2015

DOI: 10.1021/ic502815q
Inorg. Chem. 2015, 54, 2652−2659

Scheme 1. Synthetic Routes and Chemical Structures of Compounds 1 and 2

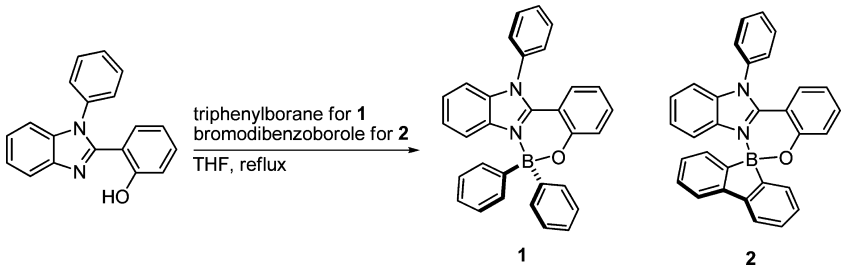

intermolecular interactions. To avoid this problem, nonconjugated structures are commonly adopted to construct deep-blue emitters. Unfortunately, most of the compounds are not efficiently emissive in the solid state because the flexible molecular structures may cause high nonirradiative transition probability. In addition, nonconjugated structures are not conducive to the carrier transport and thus may reduce the device performance. Therefore, designing novel organic materials with high charge mobility as well as intense deep-blue emission in the solid state is thus highly important and urgently demanded.

With the superiority of boron-bridged π-conjugated skeletons in constructing highly emissive materials with good charge mobility, deep-blue emissive EL boron-containing materials were synthesized by a similar design strategy. In this contribution, two novel four-coordinate boron materials **1** and **2** based on a known bidentate 2-(2-hydroxyphenyl)-benzimidazole ligand are reported. The boron chelation of triphenylborane or bromodibenzoborole with this ligand produced a rigid boron-bridged π-conjugated system, which was beneficial to both emission efficiency and charge transfer. Fundamental photophysical properties, crystal structures, and charge carrier mobility were fully investigated and discussed. To evaluate the potential of these materials in OLEDs, electroluminescent devices that employed **1** and **2** as emitters were fabricated.

RESULTS AND DISCUSSION

Material Design and Synthesis. In general, boron chelation may narrow the bandgap because of the π-conjugation extension. Thus, the ligand nature is very important for constructing wide-bandgap boron-containing materials. 2-(2-Hydroxyphenyl)benzimidazole derivatives[11] are bidentate ligands with strong coordination ability and a wide optical gap. In addition, the chelation of this type of ligand with boron moiety can produce a flat and rigid boron-bridged π-framework, which may not only intensify the emission but also enhance charge transfer. In this work, 2-(1-phenyl-1*H*-benzo[d]imidazole-2-yl)phenol (HBIZ) was employed as a ligand to synthesize two deep-blue emissive boron-containing materials in good yields (Scheme 1). Refluxing the HBIZ ligand with triphenylborane in tetrahydrofuran (THF) overnight allowed the easy synthesis of boron compound **1** as white powders. With the aim to further improve the molecular rigidity and increase the possible channel of charge transfer, molecule **2** was synthesized by the reaction of refluxing HBIZ with bromodibenzoborole. The two phenyl rings on a boron atom in compound **2** were coupled and generated a flat plane structure. Thus, compound **2** had two flat π-frameworks bridged by a boron atom, and the resulting Spiro-structure possessed three-dimensional spatial conformation with high molecular rigidity. The synthesized compounds were fully characterized by NMR, mass, element analyses, and finally X-ray crystallography diffraction. Both compounds were very stable in solution and in the solid state, as reflected by the NMR spectroscopic analyses.

Crystal Structure. To determine the molecular conformation and packing manner of compounds **1** and **2**, high quality crystals of suitable size were prepared by the solution diffusion approach and then subjected to X-ray diffraction. The colorless crystal of compound **1** takes an orthorhombic system and *Pbca* space group, and its unit cell contains a single molecule. Compound **2** crystallizes as colorless crystals with a monoclinic system and $P2_1/c$ space group. The unit cell of crystal **2** is occupied by one molecule. Figure 1 shows the molecular

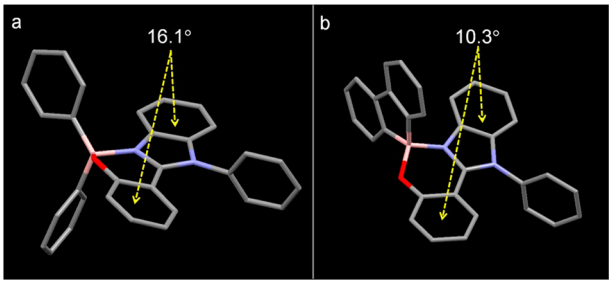

Figure 1. Crystal structures of **1** (a) and **2** (b) (hydrogen atoms are omitted for clarity).

structures of crystals **1** and **2**. The chelation of B atoms with N and O atoms produces a π-conjugated structure, and the embedded boron atoms take typical four-coordinate geometry. The dihedral angle between phenolate and benzimidazole is 16.1° for **1** and 10.3° for **2**. Thus, the boron-bridged π-framework of crystal **2** is more flat than that of **1**. The boron atoms in crystals **1** and **2** deviate from the phenolate planes by 0.61 and 0.70 Å, respectively. The lengths of the newly formed B−N and B−O bonds are comparable, being 1.595(4) and 1.506(4) Å for **1** and 1.592(2) and 1.480(2) Å for **2**. For **1**, the two peripheral phenyl rings are located above and below the boron-bridged π-plane, respectively, with maximum extension. Notably, the fused-biphenyl unit in crystal **2** is completely planar and almost perpendicular to the boron-bridged π-plane. The phenyl rings on the opposite side of boron chelation are highly twisted to the imidazole group with torsion angles of 97.1° and 84.1° for **1** and **2**, respectively.

The molecular packing structures of crystals **1** and **2** are shown in Figure 2. For **1**, each molecule interacts with another molecule through double intermolecular interactions, forming a molecular dimer. Notably, no intermolecular interactions such as π-stacking are observed for the flat, extended boron-bridged π-framework. The π-conjugated structure is effectively

DOI: 10.1021/ic502815q
Inorg. Chem. 2015, 54, 2652−2659

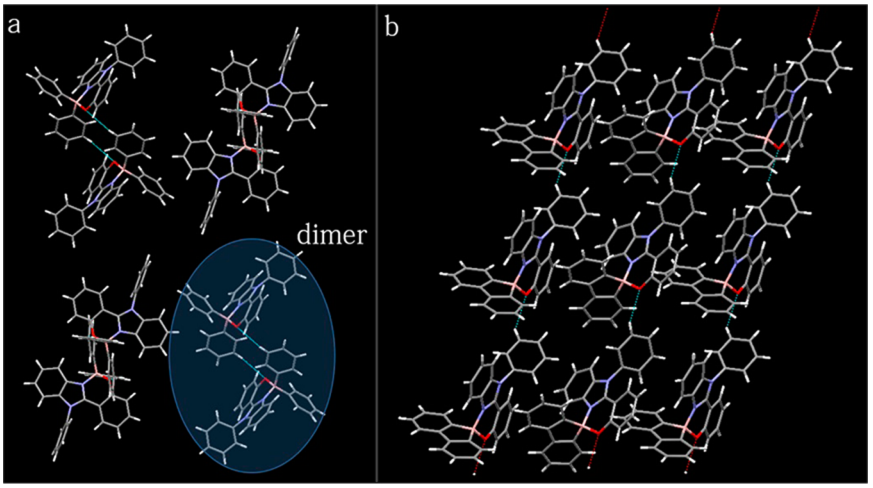

Figure 2. Crystal packing structures of compounds **1** (a) and **2** (b).

prevented from closely approaching its neighbors by the bulky side phenyl groups located above and below the boron atoms as well as the highly twisted benzene ring substituted on the imidazole unit. In crystalline **2**, an infinite one-dimensional molecular chain is formed along the crystallographic *a* direction. Similar to the structure of **1**, there are no $\pi\cdots\pi$ interactions in the molecular packing structure of **2**, although two extended π-conjugated units are found in this molecule. Thus, the luminescent units in both compounds are separated, and this feature is helpful for the π-conjugated materials to maintain high fluorescent efficiency in the solid state.

Optical Properties. The UV−vis absorption and emission properties of boron compounds **1** and **2** were measured in dichloromethane (DCM, 1×10^{-5} M), and the optical spectra are shown in Figure 3. To investigate the effect of boron

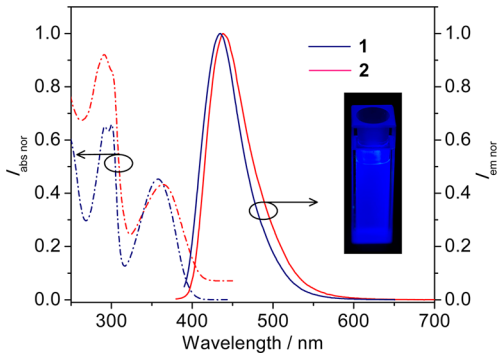

Figure 3. Optical properties of compounds **1** and **2** in CH_2Cl_2 solution (1×10^{-5} M). Inset: Photographic image of solution **1** under 365 nm irradiation.

chelation, the optical properties of the HBIZ ligand are compared. The ligand shows the longest absorption band with the peak at 322 nm in the DCM solution. Both compounds display very similar absorption profiles and the lowest energy bands, which are significantly red-shifted by 34 and 43 nm compared with the ligand. This finding might be caused by the fact that the embedded boron atom causes intramolecular electron delocalization and extends the π-conjugation skeleton. The maximum absorption peak of the longest absorption band of compound **2**, located at 365 nm, is red-shifted by approximately 10 nm compared with that of compound **1** (356 nm), indicating that the conjugation degree of the aryl substituent on the boron atom has certain effect on the absorption properties.

The HBIZ ligand is weakly emissive in DCM, showing dual emissions centered at 488 nm and a shoulder peak at around 400 nm (Figure S1, Supporting Information). Interestingly, the ligand displays two emission bands at 360 and 479 nm with comparable intensities in toluene (Figure S2, Supporting Information). The greenish blue emission band with a large Stokes shift of 9892 cm^{-1} is assigned to the excited-state intramolecular proton transfer (ESIPT), and the purple emission originates from the local emission (LE). The solution samples of boron-chelated compounds show intense deep-blue fluorescence with emission peaks at 435 nm for **1** and 438 nm for **2** in DCM and 440 nm for **1** and 446 nm for **2** in toluene. Thus, the emission spectra of compounds **1** and **2** are significantly red-shifted compared with the local emission of the ligand. The quantum yields of **1** and **2** determined by the relative method are 0.73 and 0.75, respectively, and these values are indeed high for deep-blue organic emitters. Moreover, the tails of emission bands beyond 500 nm are very weak for both compounds, which is very important for the purity of blue emissions. To fully understand the absorption and emission properties of boron compounds **1** and **2**, theoretical calculations are carried out using density functional theory (DFT) with B3LYP functional and 6-31G(d, p) basis set. The calculated data are collected in Table S2, Supporting Information, and the main electronic transitions that contribute to the absorption and emission processes are depicted in Figure 4. The calculated wavelengths at the absorption and emission peaks are consistent with the experimental measurements in DCM solution. Compounds **1** and **2** have similar absorption and emission processes, given almost the same electronic density involved in the highest occupied molecular orbitals (HOMOs) and lowest unoccupied molecular orbitals (LUMOs). The electronic transitions in the absorption and emission processes are attributed to the $\pi-\pi^*$ transitions of the HBIZ ligand and the interligand charge transfer.

Organic materials with flat π-conjugated framework usually display red-shifted absorption and emission spectra in condensed phases because of strong intermolecular interactions. Although boron compounds **1** and **2** hold flat π-planes, their solution and solid-state samples display identical optical properties. Figure 5 shows the absorption and emission spectra

DOI: 10.1021/ic502815q
Inorg. Chem. 2015, 54, 2652−2659

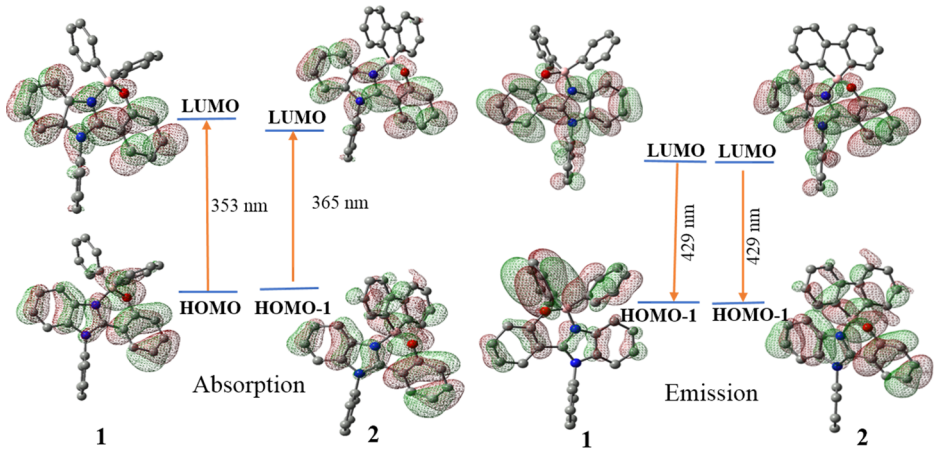

Figure 4. Main calculated electronic transitions contributing to the absorption and emission processes for compounds **1** and **2**. (Saturated H atoms are not shown.)

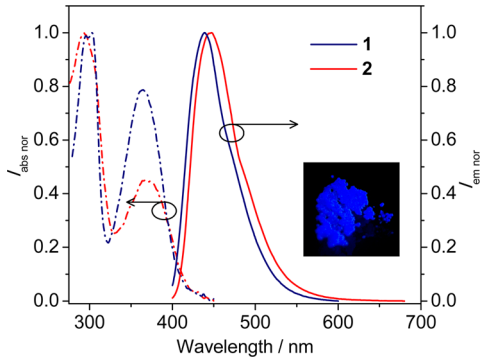

Figure 5. Optical properties of compounds **1** and **2** in vacuum deposited thin films. Inset: Photographic image of solid **1** under 365 nm irradiation.

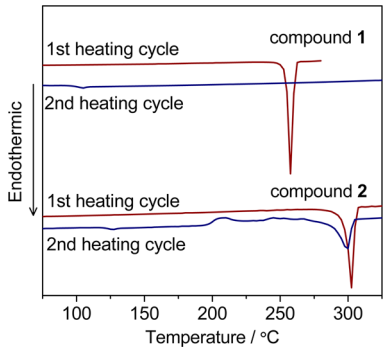

Figure 6. DSC curves of compounds **1** and **2**.

of the thin films prepared via thermal vacuum deposition. The longest absorption bands have maxima at 363 and 368 nm for compounds **1** and **2**, respectively, which are only slightly red-shifted by approximately 7 and 3 nm compared with those of the solution samples. The neat thin films or solid powders of **1** and **2** are both brightly deep-blue emissive with bands centered at approximately 440 nm, and the solid-state fluorescence quantum yields determined by an integrating sphere are 0.47 and 0.57, respectively. Thus, the synthesized boron-containing materials exhibit almost the same absorption and emission properties in dispersed (solution) and condensed (thin films and powders) phases. This observation indicates that the emissions of **1** and **2** in solid state mainly originate from the individual molecules, and intermolecular interactions like π-stacking have an insignificant effect on the emission behaviors. Notably, the majority of the solid-state emission profiles of both compounds fall within the deep-blue region because of their narrow bandwidths, which may guarantee the purity of the blue emissions.

Thermal Properties. The thermal stability of compounds **1** and **2** was evaluated by differential scanning calorimetric (DSC) and thermogravimetric analyses (TGA). As shown in Figure 6, the powder sample of compound **1** shows an intense endothermic peak at 257 °C during the first heating process, corresponding to its melt. The cooled sample displayed a small stage at approximately 104 °C when it was heated again, and no other exo- or endothermic peaks were observed. Thus, compound **1** is a good glassy material with a high glass transition temperature (T_g) of 104 °C. Similarly, the first heating process of compound **2** displays a strong endothermic peak at 301 °C, which is significantly higher than that of compound **1**. Given that compounds **1** and **2** have a similar molecular conformation and a small difference in molecular weight, the huge difference in their melting points (T_m) implies the coupling of phenyl rings indeed increases the molecular rigidity of the entire molecule. The different melting points between **1** and **2** reflect that the Spiro-structured molecule has high thermal resistance. During the second heating cycle, three obvious peaks at 126, 206, and 300 °C, which correspond to T_g, crystal transformation (T_c), and T_m, appear. The improved glass transition temperature of **2** further supports the conclusion that the compound with the fused-biphenyl structure is more thermally stable. The decomposition temperatures with a 5% weight loss for compounds **1** and **2** are 362 and 383 °C (Figure 7), respectively. Thus, the enhanced molecular rigidity improves not only the melting point but also the decomposition temperature.

Electrochemical Properties. The electrochemical properties of the boron-containing materials **1** and **2** were checked by cyclic voltammetry (CV) in DCM for oxidation and in THF for reduction. As shown in Figure 8, compounds **1** and **2** both display a reversible reduction process with half-wave potentials ($E_{red}^{1/2}$) at −2.46 and −2.40 V, respectively, presumably corresponding to the reduction of boron moieties. The potentials are close to each other, demonstrating that fusing the isolated phenyl rings on the boron atom does not change the electron-deficient nature. The oxidation waves of both

DOI: 10.1021/ic502815q
Inorg. Chem. 2015, 54, 2652−2659

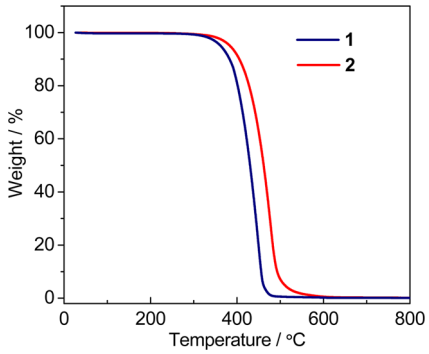

Figure 7. TGA curves of compounds **1** and **2**.

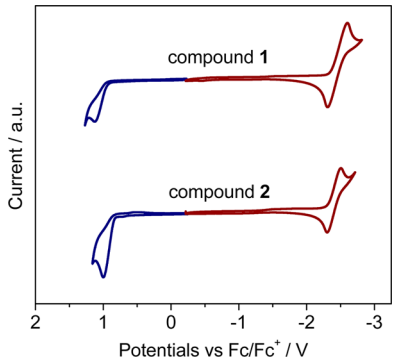

Figure 8. Cyclic voltammograms of **1** and **2** measured with $TBAPF_6$ (0.1 M) as a supporting electrolyte at a scan rate of 100 mV s^{-1}.

compounds are totally irreversible, indicating the instability of the produced radial cation. The peak potentials (E_{oxp}) are 1.14 and 1.00 V for **1** and **2**, respectively. The Spiro-structured molecule **2** displays more negatively shifted oxidation potential than compound **1**, indicating that the electron-rich nature is improved to a certain degree when the isolated phenyl rings are fused into a flat and π-conjugated structure. As a result, the bandgap of compound **2** is smaller than that of compound **1**, which matches well with the observation in the absorption spectra. The HOMO and LUMO levels based on the oxidation and reduction potentials are determined to be −5.76 and −2.34 eV for **1** and −5.65 and −2.40 eV for **2**.

Charge Mobility. High-performance nondoped OLEDs based on π-conjugated organic compounds require that the emitters have not only intense fluorescence but also balanced and high electron/hole-transporting ability. The present deep-blue emissive boron-containing materials match the requirement of high fluorescence efficiency based on the above characterization. The charge mobility of these compounds is thus carefully investigated by time-of-flight (TOF), a technique that has been widely employed to characterize charge transfer in films. Carrier-mobility measurements based on compounds **1** and **2** were carried out at room temperature with a device configuration of indium tin oxide (ITO)/compound **1** or **2** (1−2 μm)/Al (20 nm). Transient photocurrent is detected in both electron and hole mobility measurements, demonstrating that the films have an ambipolar carrier transport character (Figure 9). The electron and hole mobility values are determined to be 6.21×10^{-4} cm^2 V^{-1} s^{-1} and 2.48×10^{-4} cm^2 V^{-1} s^{-1} for **1** and 8.15×10^{-4} cm^2 V^{-1} s^{-1} and 5.82×10^{-4} cm^2 V^{-1} s^{-1} for **2** based on the equation of $\mu = D/ETt$ (where D is the thickness of the transporting layer and E is the electrical field strength) at an electric field of 1.0 MV cm^{-1}. The hole mobility of the

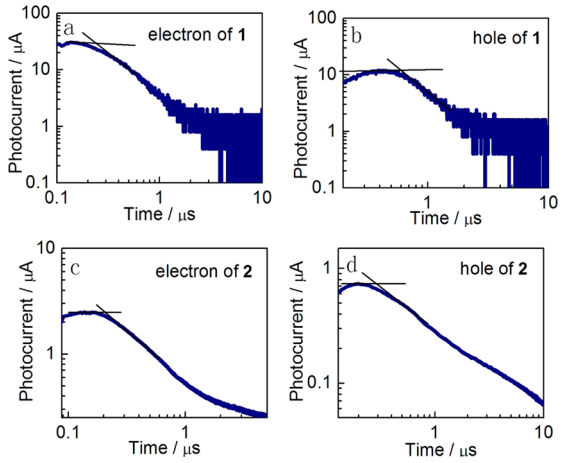

Figure 9. Hole and electron mobility of compounds **1** and **2** measured by means of TOF.

compounds is similar to that of the typical hole-transporting material *N*,*N*′-di(naphthalen-1-yl)-*N*,*N*′-diphenylbenzidine (NPB, 4.07×10^{-4} cm^2 V^{-1} s^{-1}, determined by TOF),[12] and the electron mobility is much higher than the electron-transporting material tris(8-hydroxyquinolinato)aluminum (Alq_3, 2.0×10^{-6} cm^2 V^{-1} s^{-1}, determined by TOF).[13] On the basis of these data, the film composed by compound **2** shows more balanced charge mobility than that fabricated by compound **1**.

Electroluminescent Properties. Given that these boron compounds display intense deep-blue emissions, good thermal stability, and high charge mobility, they are good candidates for constructing OLEDs. For the OLEDs devices, ITO is utilized as anode, NPB as a hole-transporting layer, and 4,4′,4″-tri(*N*-carbazoly)triphenylamine (TCTA) as an electron-blocking layer to prevent the formation of an exciplex between NPB and the boron complexes, boron complexes of **1** and **2** as emitting layers, Alq_3, 1,3,5-tris(*N*-phenylbenzimidazol-2-yl)-benzene (TPBi) and 2-(2-hydroxyphenyl)pyridine beryllium complex ($Bepp_2$) as electron-transporting layers. The electroluminescent devices employing **1** and **2** as emitters were fabricated with device configurations of ITO/NPB (30 nm)/TCTA (5 nm)/**1** (25 nm)/Alq_3 (40 nm)/LiF (1 nm)/Al (device A) and ITO/NPB(40 nm)/TCTA(5 nm)/**2** (20 nm)/TPBi(5 nm)/$Bepp_2$ (30 nm)/LiF (1 nm)/Al (device B), respectively. As shown in Figure 10, both devices A and B display blue EL with emission peaks at 440 and 445 nm,

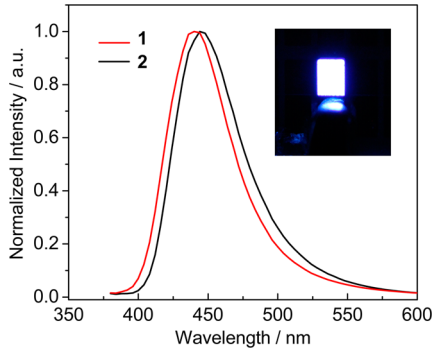

Figure 10. EL spectra of compounds **1** and **2** at 100 cd/m^2. Inset: Photographic image of device A.

DOI: 10.1021/ic502815q
Inorg. Chem. 2015, 54, 2652−2659

respectively. The EL spectra of the OLEDs based on compounds **1** and **2** are identical to the emission spectra of thin films, indicating that the EL originates from the boron emitters. In addition, the narrow bandwidth of the EL spectra allows the majority of band to fall within the deep-blue color region. As a result, the CIE coordinates (CIE_X = 0.15, CIE_Y = 0.09) for device A and (CIE_X = 0.16, CIE_Y = 0.08) for device B are close to the deep-blue emission CIE defined by the National Television System Committee (NTSC) coordinates. Therefore, the deep-blue EL that employs four-coordinate boron-containing materials is achieved. Notably, the color purity of both devices is very stable as reflected by the constant EL spectra upon increasing the driving voltage.

The performance of the two deep-blue emissive OLEDs was carefully evaluated. Device A shows a 5.0 V turn-on voltage, 2061 cd/m^2 maximum brightness, 2.80 cd/A maximum current efficiency, and 1.76 lm/W peak power efficiency. Compared with device A, device B shows improved EL performance. The turn-on voltage, brightness, maximum current efficiency, and peak power efficiency are 2.9 V, 2392 cd/m^2, 3.12 cd/A, and 3.09 lm/W, respectively. The turn-on voltage and power efficiency of device B are much better than that of device A (Figure 11), presumably because of the more balanced hole and

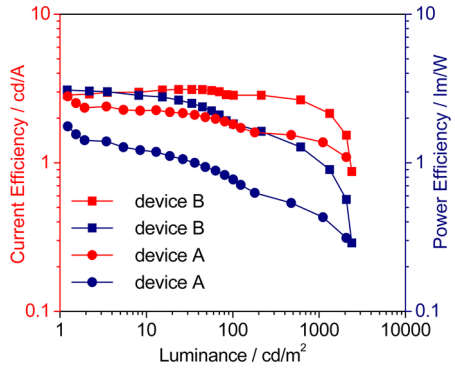

Figure 11. Efficiency-luminance characteristics of devices A and B fabricated by compounds **1** and **2**, respectively.

electron mobility of compound **2** compared with compound **1**. Device C was also fabricated with a configuration of ITO/NPB (30 nm)/TCTA (5 nm)/**1** (25 nm)/$Bepp_2$ (40 nm)/LiF (1 nm)/Al and device D with a configuration of ITO/NPB (40 nm)/TCTA (5 nm)/**2** (20 nm)/TPBi (5 nm)/Alq_3 (30 nm)/LiF (1 nm)/Al. The maximum brightness and efficiency are 805 cd/m^2 and 1.34 cd/A for device C and 1533 cd/m^2 and 1.95 cd/A for device D. The performance of devices A and B is much better than those of devices C and D. These results indicate that the electron-transporting material Alq_3 is suitable for compound **1**, whereas $Bepp_2$ is good for compound **2**.

Although many four-coordinate boron-containing materials have been constructed for fabricating OLEDs, blue emissive boron species with good EL properties is very rare. Wang and co-workers reported a N,N-chelate boron compound that can generate blue EL with a brightness and efficiency of 412 cd/m^2 and 0.83 cd/A, respectively.[4a] Our group previously fabricated blue OLEDs by employing pyridylphenolate boron compounds. These devices showed sky-blue EL with a brightness and efficiency in the range of 445−1171 cd/m^2 and 0.31−0.87 lm/W, respectively. The brightness and efficiency of the deep-blue EL devices based on the present boron compounds **1** and **2** are significantly improved compared with the blue OLEDs fabricated by other boron-containing materials.[5a]

CONCLUSIONS

Two wide-bandgap four-coordinate boron-containing materials **1** and **2** with rigid and flat π-conjugated skeleton were designed in this work. The luminescent boron-bridged π-planes in both molecules are prevented from closely approaching its neighbors by the phenyl substituents on the boron atom and the imidazole group. Thus, both boron compounds display highly efficient deep-blue emissions in solution and solid phases with narrow bandwidths. In addition, these two materials exhibit good thermal stability and high ambipolar transporting properties. Compared with **1**, molecule **2** with fused-biphenyl π-skeletons not only increases the thermal stability but also enhances the charge mobility and thus performs better in electroluminescent device. OLEDs that employ **1** and **2** as emitting materials show deep-blue EL with CIE_Y below 0.10. The present study not only provides boron-containing materials with high-performance deep-blue EL but also gives an indication of design principles toward efficient wide-bandgap boron-containing emitters.

EXPERIMENTAL SECTION

General Information. All starting materials and solvents were purchased from commercial sources. The solvents for syntheses were freshly distilled over appropriate drying reagents. All experiments were performed under a nitrogen atmosphere using standard Schlenk techniques. ^{1}H NMR, ^{13}C NMR were measured on Bruker Avance 500 MHz spectrometer with tetramethylsilane (TMS) as internal standard. Mass spectra were recorded on GC/MS mass spectrometer. Elemental analyses were performed on a Vario Micro (Elementar) spectrometer. UV−vis absorption spectra were recorded by a Shimadzu UV-2550 spectrophotometer. The emission spectra were recorded by a Shimadzu RF-5301 PC spectrometer. Cyclic voltammetries were performed on a BAS 100W instrument with a scan rate of 100 mV s^{-1}. A three-electrode configuration was used for the measurement: a platinum electrode as the working electrode, a platinum wire as the counter electrode, and an Ag/Ag$^+$ electrode as the reference electrode. A 0.1 M solution of tetrabutylammonium hexafluorophosphate (TBAPF) in CH_2Cl_2 or THF was used as the supporting electrolyte. Differential scanning calorimetric (DSC) measurements were performed on a NETZSCH DSC204 instrument at a heating rate of 10 °C min^{-1} under nitrogen. Thermogravimetric analyses (TGA) were performed on a TAQ500 thermogravimeter at a heating rate of 10 °C min^{-1} under nitrogen.

Single Crystal Structure. Single crystal X-ray diffraction data were collected on a Rigaku RAXIS-PRID diffractometer using the ω-scan mode with graphite-monochromator Mo·Kα radiation. The structures were solved with direct methods using the SHELXTL programs[14] and refined with full-matrix least-squares on F^2. Non-hydrogen atoms were refined anisotropically. The positions of hydrogen atoms were calculated and refined isotropically.

Photoluminescent (PL) Quantum Yield Measurements. The solution fluorescence quantum yields were measured in dilute CH_2Cl_2 relative to quinine sulfate in sulfuric acid aqueous solution (λ_{ex} = 365 nm, Φ_F = 0.546) at room temperature. The quantum yields were calculated using previously known procedures.[15] The solid-state quantum yields were measured using an integrating sphere with the excitation wavelength of 365 nm for both compounds.

Device Fabrication. ITO-coated glass was used as the substrate. It was cleaned by sonication successively in a detergent solution, acetone, methanol, and deionized water before use. The devices were prepared in a vacuum at a pressure of 5 × 10^{-4} Pa. Organic layers were deposited onto the substrate at a rate of 0.3−0.5 Å/s. After the organic film deposition, LiF and aluminum were thermally evaporated onto the organic surface. The thicknesses of the organic materials and the

DOI: 10.1021/ic502815q
Inorg. Chem. 2015, 54, 2652−2659

cathode layers were controlled using a quartz crystal thickness monitor. The electrical characteristics of the devices were measured with a Keithley 2400 sourcemeter. The EL spectra and luminance of the devices were obtained on a PR650 spectrometer. All measurements of the devices were carried out in ambient atmosphere without further encapsulations.

Computational Details. Ab initio calculations were carried out with the Gaussian 09 package.[16] Geometries at the ground states for complexes **1** and **2** were optimized with the density functional theory (DFT) using the B3LYP functional and 6-31G** basis set. The geometries optimization at the first singlet excited state were carried out with time-dependent density functional theory (TD-DFT) at the same level of theory. The optimized geometries were confirmed to be potential energy minima by frequency calculation at the same level of theory, as a complete set of real frequencies were found. The vertical excitations were performed with TD-DFT methods for iteratively solving 20 states at the optimized geometries in the ground and excited states to simulate the absorption and emission processes. Solvent effects were taken into account by the polarizable continuum model (PCM) with dichloromethane as solvent for comparing with the photophysical data with experimental measurements.

Synthesis and Characterization. The precursor bromodibenzoborole reagent was synthesized following the reported literature reports.[17] Mixtures of the ligand and the organoborane reagents were refluxed in THF for 12 h, and subsequent purification by vacuum sublimation produced the final compounds in high yields. All the newly synthesized boron complexes were fully characterized by NMR, mass spectra, and elemental analysis.

Compound **1**. Yield: 70%. ^{1}H NMR (DMSO, 500 MHz, ppm): δ 7.88−7.72 (m, 5 H), 7.43−7.28 (m, 6 H), 7.24 (t, J = 7.5 Hz, 1 H), 7.13−7.21 (m, 7 H), 7.10 (d, J = 8.5 Hz, 1 H), 9.83 (d, J = 8.5 Hz, 1 H), 6.61 (d, J = 8.0 Hz, 1 H), 6.52 (t, J = 7.5 Hz, 1 H). ^{13}C NMR ($CDCl_3$, 500 MHz, ppm): δ 162.4, 149.0, 146.5, 135.5, 135.2, 134.5, 134.4, 133.4, 130.8, 130.7, 127.8, 127.2, 126.3, 126.2, 125.0, 124.7, 121.4, 117.9, 117.5, 110.9, 110.6. Elemental analysis: found C, 82.85%; H, 5.10%; N, 6.31%; calc. for $C_{31}H_{23}BN_2O$: C, 82.68%; H, 5.15%; N, 6.22%. MS m/z: 450.3 [M^+] (calcd: 450.2).

Compound **2**. Yield: 78%. ^{1}H NMR ($CDCl_3$, 500 MHz, ppm): δ 7.79−7.72 (m, 5 H), 7.55−7.61 (m, 2 H), 7.29−7.40 (m, 5 H), 7.20 (t, J = 7.5 Hz, 1 H), 7.16(d, J = 8.5 Hz, 1 H), 7.10−7.02 (m, 4 H), 6.84 (dd, J = 4.0 Hz, J = 1.5 Hz, 1 H), 6.60−6.68 (m, 2 H). ^{13}C NMR ($CDCl_3$, 500 MHz, ppm): δ 162.7, 151.0, 148.8, 146.6, 135.5, 135.2, 134.5, 132.9, 130.9, 130.8, 130.1, 128.1, 127.8, 126.7, 125.9, 125.2, 125.0, 121.5, 119.4, 118.3, 116.8, 110.7, 110.6. Elemental analysis: found C, 83.21%; H, 4.66%; N, 6.35%; calc. for $C_{31}H_{21}BN_2O$: C, 83.05%; H, 4.72%; N, 6.25%. MS m/z: 448.3 [M^+] (calcd: 448.2).

■ ASSOCIATED CONTENT

Ⓢ Supporting Information

Listings of some spectra, tables, crystallographic data in PDF and cif format, molecular structures of auxiliary OLED materials, and NMR spectra. This material is available free of charge via the Internet at http://pubs.acs.org.

■ AUTHOR INFORMATION

Corresponding Authors

*(J.Z.) E-mail: zhangjingy@jlu.edu.cn.

*(H.Z.) E-mail: hongyuzhang@jlu.edu.cn.

Notes

The authors declare no competing financial interest.

■ ACKNOWLEDGMENTS

This work was supported by the National Basic Research Program of China (2013CB834805), the National Natural Science Foundation of China (51173067 and 91333201) and Program for Chang Jiang Scholars and Innovative Research Team in University (No. IRT101713018).

■ REFERENCES

(1) For recent reviews see: (a) Figueira-Duarte, T. M.; Müllen, K. *Chem. Rev.* **2011**, *111*, 7260. (b) Anthony, J. E. *Chem. Rev.* **2006**, *106*, 5028. (c) Saragi, T. P. I.; Spehr, T.; Siebert, A.; Fuhrmann-Lieker, T.; Salbeck, J. *Chem. Rev.* **2007**, *107*, 1011. (d) Hudson, Z. M.; Wang, S. *Acc. Chem. Res.* **2009**, *42*, 1584. (e) Zhao, Y. S.; Fu, H.; Peng, A.; Ma, Y.; Liao, Q.; Yao, J. *Acc. Chem. Res.* **2010**, *43*, 409. (f) Tatum, L. A.; Su, X.; Aprahamian, I. *Acc. Chem. Res.* **2014**, *47*, 2141. (g) Fukazawa, A.; Yamaguchi, S. *Chem.—Asian J.* **2009**, *4*, 1386.

(2) (a) Rao, Y.-L.; Wang, S. *Inorg. Chem.* **2011**, *50*, 12263. (b) Li, D.; Yuan, Y.; Bi, H.; Yao, D.; Zhao, X.; Tian, W.; Wang, Y.; Zhang, H. *Inorg. Chem.* **2011**, *50*, 4825. (c) Madhu, S.; Ravikanth, M. *Inorg. Chem.* **2012**, *51*, 4285. (d) Lifschitz, A. M.; Shade, C. M.; Spokoyny, A. M.; Mendez-Arroyo, J.; Stern, C. L.; Sarjeant, A. A.; Mirkin, C. A. *Inorg. Chem.* **2013**, *52*, 5484. (e) Sarkar, S. K.; Mukherjee, S.; Thilagar, P. *Inorg. Chem.* **2014**, *53*, 2343. (f) Zhang, Z.; Bi, H.; Zhang, Y.; Yao, D.; Gao, H.; Fan, Y.; Zhang, H.; Wang, Y.; Wang, Y.; Chen, Z.; Ma, D. *Inorg. Chem.* **2009**, *48*, 7230.

(3) (a) Yoshii, R.; Hirose, A.; Tanaka, K.; Chujo, Y. *Chem.—Eur. J.* **2014**, *20*, 8320. (b) Xu, S.; Evans, R. E.; Liu, T.; Zhang, G.; Demas, J. N.; Trindle, C. O.; Fraser, C. L. *Inorg. Chem.* **2013**, *52*, 3597. (c) Galer, P.; Korošec, R. C.; Vidmar, M.; P. Šket, B. *J. Am. Chem. Soc.* **2014**, *136*, 7383. (d) Nagai, A.; Kokada, K.; Nagata, Y.; Chujo, Y. *Macromolecules* **2008**, *41*, 8295. (e) Nagai, A.; Kokado, K.; Nagata, Y.; Arita, M.; Chujo, Y. *J. Org. Chem.* **2008**, *73*, 8605. (f) Zhang, G.; Lu, J.; Sabat, M.; Fraser, C. L. *J. Am. Chem. Soc.* **2010**, *132*, 2160.

(4) (a) Liu, Q.-D.; Mudadu, M. S.; Thummel, R.; Tao, Y.; Wang, S. *Adv. Funct. Mater.* **2005**, *15*, 143. (b) Liddle, B. J.; Silva, R. M.; Morin, T. J.; Macedo, F. P.; Shukla, R.; Lindeman, S. V.; Gardinier, J. R. *J. Org. Chem.* **2007**, *72*, 5637. (c) Curiel, D.; Más-Montoya, M.; Usea, L.; Espinosa, A.; Orenes, R. A.; Molina, P. *Org. Lett.* **2012**, *14*, 3360.

(5) (a) Zhang, H.; Huo, C.; Ye, K.; Zhang, P.; Tian, W.; Wang, Y. *Inorg. Chem.* **2006**, *45*, 2788. (b) Zhang, H.; Huo, C.; Zhang, J.; Zhang, P.; Tian, W.; Wang, Y. *Chem. Commun.* **2006**, 281. (c) Zhang, Z.; Yao, D.; Zhao, S.; Gao, H.; Fan, Y.; Su, Z.; Zhang, H.; Wang, Y. *Dalton Trans.* **2010**, *39*, 5123.

(6) (a) Cui, Y.; Liu, Q.-D.; Bai, D.-R.; Jia, W.-L.; Tao, Y.; Wang, S. *Inorg. Chem.* **2005**, *44*, 601. (b) Qin, Y.; Kiburu, I.; Shah, S.; Jäkle, F. *Org. Lett.* **2006**, *8*, 5227. (c) Cui, Y.; Wang, S. *J. Org. Chem.* **2006**, *71*, 6485. (d) Qin, Y.; Pagba, C.; Piotrowiak, P.; Jäkle, F. *J. Am. Chem. Soc.* **2004**, *126*, 7015.

(7) (a) Wakamiya, A.; Taniguchi, T.; Yamaguchi, S. *Angew. Chem., Int. Ed.* **2006**, *45*, 3170. (b) Son, H.-J.; Han, W.-S.; Wee, K.-R.; Chun, J.-Y.; Choi, K.-B.; Han, S. J.; Kwon, S.-N.; Ko, J.; Lee, C.; Kang, S. O. *Eur. J. Inorg. Chem.* **2009**, 1503.

(8) (a) Job, A.; Wakamiya, A.; Kehr, G.; Erker, G.; Yamaguchi, S. *Org. Lett.* **2010**, *12*, 5470. (b) Fukazawa, A.; Yamada, H.; Yamaguchi, S. *Angew. Chem., Int. Ed.* **2008**, *47*, 5582. (c) Kubota, Y.; Tanaka, S.; Funabiki, K.; Matsui, M. *Org. Lett.* **2012**, *14*, 4682. (d) Kubota, Y.; Hara, H.; Tanaka, S.; Funabiki, K.; Matsui, M. *Org. Lett.* **2011**, *13*, 6544. (e) Wu, Y.-Y.; Chen, Y.; Gou, G.-Z.; Mu, W.-H.; Lv, X.-J.; Du, M.-L.; Fu, W.-F. *Org. Lett.* **2012**, *14*, 5226. (f) Cheng, X.; Li, D.; Zhang, Z.; Zhang, H.; Wang, Y. *Org. Lett.* **2014**, *16*, 880.

(9) Li, D.; Zhang, H.; Wang, Y. *Chem. Soc. Rev.* **2013**, *42*, 8416.

(10) (a) Liddle, B. J.; Silva, R. M.; Morin, T. J.; Macedo, F. P.; Shukla, R.; Lindeman, S. V.; Gardinier, J. R. *J. Org. Chem.* **2007**, *72*, 5637. (b) Massue, J.; Frath, D.; Ulrich, G.; Retailleau, P.; Ziessel, R. *Org. Lett.* **2012**, *14*, 230. (c) Benelhadj, K.; Massue, J.; Retailleau, P.; Ulrich, G.; Ziessel, R. *Org. Lett.* **2013**, *15*, 2918. (d) Dijkstra, P.; Angelone, D.; Talnishnikh, E.; Wörtche, H. J.; Otten, E.; Browne, W. R. *Dalton Trans.* **2014**, *43*, 17740.

(11) (a) Thiruvalluvar, A.; Rosepriya, S.; Jayamoorthy, K.; Jayabharathi, J.; ÖztürkYildirim, S.; Butcher, R. J. *Acta. Crystallogr. Sect. E* **2013**, *69*, o62. (b) Esparza-Ruiz, A.; Peña-Hueso, A.; Nöth, H.; Flores-Parra, A.; Contreras, R. J. *Organomet. Chem.* **2009**, *694*, 3814. (c) Ju, C.-C.; Zhang, A.-G.; Sun, H.-L.; Wang, K.-Z. *Organometallics* **2011**, *30*, 712.

(12) Tse, S. K.; Tsang, S. W.; Tsang, S. W.; So, S. K. *Proc. SPIE* **2006**, *6333*, 63331P.

DOI: 10.1021/ic502815q
Inorg. Chem. 2015, 54, 2652−2659

(13) (a) Malliaras, G. G.; Shen, Y.; Dunlap, D. H.; Murata, H.; Kafafi, Z. H. *Appl. Phys. Lett.* **2001**, *79*, 2582. (b) Tsai, T.-C.; Hung, W.-Y.; Chi, L.-C.; Wong, K.-T.; Hsieh, C.-C.; Chou, P.-T. *Org. Electron.* **2009**, *10*, 158.
(14) (a) *SHELXTL*, version 5.1; Siemens Industrial Automation, Inc.: Berlin, 1997. (b) Sheldrick, G. M. *SHELXS-97, Program for Crystal Structure Solution*; University of Göttingen: Göttingen, 1997.
(15) Ye, K.; Wang, J.; Sun, H.; Liu, Y.; Mu, Z.; Li, F.; Jiang, S.; Zhang, J.; Zhang, H.; Wang, Y.; Che, C. M. *J. Phys. Chem. B* **2004**, *109*, 8008.
(16) Frisch, M. J.; Trucks, G. W.; Schlegel, H. B.; Scuseria, G. E.; Robb, M. A.; Cheeseman, J. R.; Scalmani, G.; Barone, V.; Mennucci, B.; Petersson, G. A.; Nakatsuji, H.; Caricato, M.; Li, X.; Hratchian, H. P.; Izmaylov, A. F.; Bloino, J.; Zheng, G.; Sonnenberg, J. L.; Hada, M.; Ehara, M.; Toyota, K.; Fukuda, R.; Hasegawa, J.; Ishida, M.; Nakajima, T.; Honda, Y.; Kitao, O.; Nakai, H.; Vreven, T.; Montgomery, J.; Peralta, J. E.; Ogliaro, F.; Bearpark, M.; Heyd, J. J.; Brothers, E.; Kudin, K. N.; Staroverov, V. N.; Kobayashi, R.; Normand, J.; Raghavachari, K.; Rendell, A.; Burant, J. C.; Iyengar, S. S.; Tomasi, J.; Cossi, M.; Rega, N.; Millam, J. M.; Klene, M.; Knox, J. E.; Cross, J. B.; Bakken, V.; Adamo, C.; Jaramillo, J.; Gomperts, R.; Stratmann, R. E.; Yazyev, O.; Austin, A. J.; Cammi, R.; Pomelli, C.; Ochterski, J. W.; Martin, R. L.; Morokuma, K.; Zakrzewski, V. G.; Voth, G. A.; Salvador, P.; Dannenberg, J. J.; Dapprich, S.; Daniels, A. D.; Farkas, O.; Foresman, J. B.; Ortiz, J. V.; Cioslowski, J.; Fox, D. J. *Gaussian 09*, Revision A.01; Gaussian, Inc.: Wallingford, CT, 2009.
(17) (a) Wakamiya, A.; Mishima, K.; Ekawa, K.; Yamaguchi, S. *Chem. Commun.* **2008**, *5*, 279. (b) Gross, U.; Kaufmann, D. *Chem. Ber.* **1987**, *120*, 991.

DOI: 10.1021/ic502815q
Inorg. Chem. 2015, 54, 2652−2659